Molecular docking analysis and anti-apoptotic activity of Hypericum triquetrifolium Turra (St. John's-wort) in Cyclophosphamide-induced lung injury

Songül Çetik Yıldız
Mardin Artuklu University: T C Mardin Artuklu Universitesi
Cumali Keskin
Mardin Artuklu University: T C Mardin Artuklu Universitesi
Varol Şahintürk
Osmangazi University: Eskisehir Osmangazi Universitesi
Bahri Gür
Iğdır Üniversites: Igdir Universitesi
Yasemin Oğul
Erzurum Training and Research Hospital: Erzurum Bolge Egitim ve Arastirma Hastanesi
Mustafa CENGİZ (mustafacengizogu@gmail.com)
Siirt Universitesi https://orcid.org/0000-0002-6925-8371
Adnan Ayhanci
Osmangazi University: Eskisehir Osmangazi Universitesi

Research Article

Keywords: Hyperoside, Cyclophosphamide, immunohistochemical, Lung Tissues, histopathological, Negative Binding Energy, and Affinity

Posted Date: August 16th, 2022

DOI: https://doi.org/10.21203/rs.3.rs-1919227/v1

Abstract

The present study aims to investigate the lung-protective and antiapoptotic effects of *Hypericum triquetrifolium Turra* (HTT) against cyclophosphamide (CP)-induced lung injury in rats. Thirty-five Sprague Dawley rats were categorized into 5 groups, each consisting of seven members. Phenolic acid and flavonoid contents of this plant were determined. The lung tissue samples cultivated from the rats were examined both histopathological and immunohistochemically for the apoptosis markers of Caspase-3, Bax, and Bcl-2. Histopathological results indicated that structural defects, bleeding areas, and edema had occurred in the lungs of the CP-Alone Group. Besides, Caspase-3 and Bax positivity of the lung cells had also increased while Bcl-2 positivity had decreased. On the other hand, in the HTT + CP Group, HTT was shown to have reversed the aforementioned changes positively. In addition, our *in-vivo* results were confirmed by the *in-silico* studies. The changes that occurred in the binding of CP to the active-site amino acid residues of Caspase-3, Bax, and Bcl-2 upon the addition of Hyperoside besides the changes that occurred in their tendency to form hydrogen bonds were accounted for by *in silico* studies. Based on *in vivo* and *in silico* results, HTT could be a strong protective candidate for CP-induced lung injury and apoptosis.

Introduction

The lung is vulnerable to the detrimental effects of various xenobiotics, such as drugs, natural toxins, and environmental pollutants (Abdel-Latif et al., 2020). Alkylating antineoplastic groups of drugs are potent drugs that can damage the balance of antioxidant-oxidants (Saghir et al., 2020). Cyclophosphamide (CP) is an oxazaphosphorine derivative of alkylating nitrogen mustard typically used as a chemotherapeutic drug in treating cancer (Abd El-Ghafar et al., 2021). Studies showing damage to healthy tissues due to CP, including the kidney, the liver and the lung, and the testis, have limited the application of this drug for treating cancer (Badawi, 2022; Cengiz et al., 2019).

Inadequacy of detoxifying enzymes in the lung tissue is accepted to be the main reason for lung toxicity caused by CP (Mohamed et al., 2020). It has been reported that CP exposure causes deterioration of redox balance after oxidative stress causing biochemical and physiological disturbances (Cengiz et al., 2020; Das et al., 2002). CP is a generally prescribed anticancer drug applied in the treatment of various neoplastic diseases. Cytotoxic effects of CP are due to chemically reactive metabolites that produce cross-linking, which alkylate DNA and protein (Habibi et al., 2020). Reactive oxygen species (ROS) have essential roles in the pathogenesis of acute and chronic lung damage. Because oxygen is vital for living, the cells that cover the airways and the surface area of the alveolus always need oxygen. Known as pulmonary defense cells, neutrophils, monocytes, and macrophages tend to be effectively inclined to convert molecular oxygen to ROS (El-Kashef, 2018; Naraoka et al., 2021). Studies have shown CP to cause inflammatory reactions in the lungs of rats apart from causing acrolein/ROS formation, increasing lipid peroxidation, and accumulating neutrophils while the drug is being metabolized (Abd El-Ghafar et al., 2021).

Species of Hypericum, also known as the Clusioid clade, belong to the Hypericaceae family (Silva et al., 2021). There are known to be many bioactive compounds in the methanolic extracts of Hypericum species (Can et al., 2022; Chen et al., 2021). A member of the Hypericaceae family, HTT has been traditionally used in medical treatments due to its sedative, antiseptic, anti-inflammatory, and anthelmintic properties (Ibaokurgil et al., 2022). Furthermore, HTT has flavonoid and phenolic compounds with such properties as chlorogenic acid, hyperoside, quercitrin, quercetin, and routine apart from having antioxidant properties (Manzullo & Escalante, 2002; Toker, 2009). Besides, the antioxidant property of HTT helps to prevent or reduce the progression of many oxidative stress-mediated diseases (Can et al., 2022). The effect of such compounds on the activity of biomolecules is evaluated by taking into consideration the hydrogen bonding and other interactions that occur between the biomolecules and the ligand.

Being of great significance for biomolecules, hydrogen bonds formed over -NH and -OH groups in biomolecules significantly affect the shape and function of the biomolecule. They are also essential for enzymatic catalysis in stabilizing a ligand in a binding pocket (Kostal, 2016). As far as biomolecule-ligand interactions are concerned, the number and length of hydrogen bonds and such interactions as carbon-hydrogen, van der Waals, Donor-Donor interactions, and Pi-Alkyl that ligand forms with the active site amino acid residues of the biomolecule decrease the value of the free energy value resulting from biomolecule -ligand interactions. This decrease is typically regarded as an indicator of the protein's affinity to the ligand (Canofeni et al., 1994; Gür, 2020; Shityakov & Förster, 2014). All these taken into account, the present study investigates whether the protective effects of HTT extract can decrease CP-induced toxicity on the lung tissue of rats thanks to *in vivo* and *in silico* studies.

Materials And Methods

Drug and chemicals

Endoxan, Cyclophosphamide Monohydrate, and C0768 (CP) were commercially obtained from Sigma-Aldrich, Taufkirchen, Germany. 500 mg CP was dissolved in bi-distilled water (25 mL) before being injected into the rats, each of them given a single dose of 150 mg/kg of CP intraperitoneally.

Plant Extraction

Samples of HTT were collected during the seeding periods (between August and September 2015), which were then stored in the herbarium of Mardin Artuklu University. Afterward, 20 g of seed powder was extracted three times using 200 ml of absolute methanol, upon which 4.0 g of crude extract was obtained and then stored at -20ºC prior to the onset of the experiment. Next, this extract was dissolved with 0.2% dimethyl sulfoxide (DMSO) to produce 100 mg/kg HTT. It was filtered for high-performance liquid chromatography (HPLC) via a membrane filter with a pore of 0.22 µm (Carl Roth GmbH, Karlsruhe, Germany). HPLC analyses of phenolic acid and flavonoid were performed using a Waters model 2690 gradient pump with Waters 2487 UV detector and XTerra RP18 column (150 Å~ 3.9 mm, 3.5 µm)(Alzoubi et al., 2020; Mustafa & Maulood, 2019).

Animals

Male Sprague Dawley rats were provided from the Experimental Animals Lab. Ind. Trade. Corp. Co., which received approval from the Experimental Animal Ethics Committee of Eskişehir Osmangazi University (Protocol No. 444-1/2015). 220 ± 20 g healthy, 3-4 months old male rats were kept in normal environmental conditions, including 25 ± 2 °C room temperature, 60-70%, humidity, and 12 h light-dark cycles. Care was taken to make sure that these animals could reach standard pellet feed and water easily.

Experimental Groups

Five groups of seven rats each were formed from the 35 total animals. Group 1 (the control) received 0.5 mL of saline, Group 2 was given 150 mg/kg of CP, and Groups 3 was administrated 100 mg/kg of HTT. Groups 4 received HTT+CP, and Group 5 received 0.2 mL of DMSO (% 0.2).

Chemical and medication dosages were chosen and prepared for the injection. Every injection was intraperitoneal (i.p). Group 1: Control rats received 0.5 ml of so-called normal saline (SF) over 6 days. Group 2 rats received SF treatment for five days before receiving a single dosage of CP on the sixth day. For six days, rats in Group 3 received the appropriate HTT-dose treatment. Rats in Group 4 received the appropriate dose of HTT. A single dose of CP was given on the sixth day. Group 5 received % 0.2 DMSO treatment for 6 days. Blood samples were collected through heart puncture under ketamine/xylazine anesthesia to evaluate serum parameters before the animals were euthanized on the seventh day (Table 1).

Table 1: The protocol devised for all the study groups and the chemicals used

Groups	Treatment	Number of animals
Control	Control (saline i.p.)	7
CP	150 mg/kg	7
HTT	100 mg/kg	7
CP + HTT	150 mg/kg + 100 mg/kg	7
DMSO	0.2% (0.2 mL)	7

Histological Examination

Lungs from experimental albino rats were processed using an automated tissue processor after being formalin-preserved. Dehydration and fixation served as the processing's first two steps. During fixation, the tissue is submerged for 48 hours in 10 percent buffered formalin before the fixative is washed away with distilled water for 30 minutes. After that, the tissues were given two cycles of 100 percent alcohol for one hour each in order to dehydrate them. Initially, the tissues were exposed to 70% alcohol for 120 minutes, then to 90% alcohol for 90 minutes. After dehydration, the samples were cleaned in multiple

xylene changes. During the operation, tissue was submerged for one hour in a mixture of 50% xylene and 50% alcohol, then for another 1.5 hours in pure xylene. The samples were then impregnated with molten paraffin wax, blacked out, and embedded (Suvarna et al., 2018). Slices made from 4-5 M paraffin were stained using hematoxylin and eosin. Following conventional HE staining, morphological parameters were evaluated using light microscopy. A pathologist who was unaware of the groups evaluated lung injury using histological abnormalities like alveolar congestion, alveolar wall edema, inflammatory cell infiltration, and bleeding.

The pathologist also recorded the histopathology grade for the tissues in the left lung, which was based on the aforementioned reference (Liu et al., 2019). Each benchmark was rated between 0 (normal) and 4 (severe), where 0 indicates no harm or a very minor injury, 1, 2, 3, and 4 are mild, serious, medium, and extremely serious injuries, respectively. The diffuse alveolar injury standard (DAS) score is the name of this approach. The sum of all scores was used to establish the overall score for the pathology of lung tissues.

Immunohistochemistry Examination

The 5-m sections were deparaffinized, rehydrated, and subjected to antigen retrieval using a variety of newly discovered methods. The samples were cleaned with PBS and then blocked with 10% goat serum. The primary antibody (1:500; anti-Bax, anti-caspase-3, and anti-Bcl-2 antibody; Abcam, Cambridge, UK) was incubated with the samples for 24 hours at 40°C. After washing the samples, the secondary antibody was incubated with them for 90 minutes at room temperature (1:1500; goat anti-rabbit IgG; Abcam). The slides were examined using the Leica DM500 Biological Microscope after the samples had been cleaned (Caspase-3 (Thermo Fischer), Bcl-2 (Abcam), and Bax (Abcam)).

Molecular modeling studies of the interactions of CP, HTT, CPM+HTT with Caspase-3, Bax, and Bcl-2 macromolecules

The *in silico* studies conducted in the present study aimed to determine the interactions between CP, HTT, CP+HTT with Caspase-3, Bax, and Bcl-2 respectively, as well as revealing the possible mechanisms of these interactions and the binding sites preferred across the proteins by CP, HTT and CP+HTT using PyRx version 0.8 and Discovery Studio 3.0 (Accelrys Inc., San Diego, USA) programs. Downloaded were the crystal structures of Caspase-3, Bax, and Bcl-2 macromolecules from the RSCB Protein Databank, the PDB codes of which were 1GFW, 1F16, and 2O2F, respectively. All the active site amino acid residues (ASAR) of the macromolecules used in this study were determined using the Discovery Studio Visualizer program and the results of previous studies (Cheemanapalli et al., 2018; Kaya et al., 2021; Siddiqui et al., 2021; Sinha & Vidyarthi, 2011).

The ASARs identified for Caspase-3 were Phe256, Arg207, Gls206, Ser205, Tyr204, Cys163, Gly122, His121, Met61, Ser58, and Lys57, whereas those identified for Bax were Met20, Ala24, Leu27, Ile31, Ile133, Met137, and Leu141 in addition to a perimeter of charged and hydrophilic residues, including Lys21,

Gln28, Gln32, Glu131, and Arg134. As for the ASARs identified for Bcl-2, they were found to be Ala97, Asp100, Tyr105, Asp108, Met112, Val130, Leu134, Trp141, Gly142, Val145, Ala146, and Tyr199.

Not only the molecular models of CP but also HT molecules with an SDF form were downloaded from the PubChem database website, the SDF codes of which were Structure2D_CID_2907, and Structure2D_CID_5281643, respectively. The dockings of CP and HT into the active site of Caspase-3, Bax, and Bcl-2 were performed thanks to the PyRx program (Gür, 2020; Gür, Cengiz, Kutlu, et al., 2021; Trott & Olson, 2010). The energy minimization and the other parameters were set as done in our previous studies (Gür, Cengiz, & Gür, 2021; Gür et al., 2020).

Nine different binding modes were opted to find out which residues of Caspase-3, Bax, and Bcl-2 the CP and HT molecules tended to bind thanks to the PyRx program, upon which both CP and HT molecules used were adjusted so that they would be compatible with the Discovery Studio 3.0 program to be used as a ligand. Subsequently, the interactions of Caspase-3, Bax, and Bcl-2 macromolecules with CP and HT molecules were exposed with the aid of 2D and 3D interaction modes. As for the negative binding energy parameters, they were determined considering the lowest free energy values.

Statistical Examination

The findings were defined as means ± S.E.M. The statistical analyses used were One Way Analysis of Variance and Kruskal-Wallis One Way Analysis of Variance on Ranks Test. The data obtained for the contents of the plant seed material were subjected to ANOVA. Each of the experiments was repeated three times.

Results

Lung tissue samples cultivated from the rats were not only histopathologically but also immunohistochemically analyzed for Bax, Bcl-2, and Caspase-3 on a routine basis.

Content of the seed of Hypericum triquetrifolium

The levels of all the compounds detected in Hypericum triquetrifolium were hyperoside (HT), kaempferol, quercetin, quercitrin, rutin, amentoflavone, chlorogenic acid, and apigenin-7-O-glucoside were examined and presented in Table 2. Considering this table, the compound with the largest amount of *Hypericum triquetrifolium* was determined to be that of Hyperoside (HT) (8.42 mg/g DW).

Table 2. Compounds available in *Hypericum triquetrifolium* (mg/g DW)

Compounds	H. triquetrifolium
Hyperoside (HT)	**8.42**
Kaempferol	0.02
Quercetin	1.91
Quercitrin	2.76
Rutin	3.72
Amentoflavone	0.006
Chlorogenic acid	2.07
Apigenin-7-O-glucoside	0.14

Histological Evaluations

Lung tissues of the experimental groups (Control, 0.2% DMSO, and 100 mg/kg HTT) had all normal histology as presented in Table 2, Figure 1/A. Serious damage was observed in the lung tissues of the rats injected CP (150 mg/kg), including structural defects, obstruction, edema foci, bleeding areas, and alveolar cell injuries, as presented in Table 3, Figure 2/A. However, this damage greatly improved in the group injected CP+HTT as presented in Table 2, Figure 3/A.

Apoptotic Evaluations

The lung tissue samples of Control, CP, HTT, CP + HTT, and DMSO groups were immunohistochemically stained to determine the density and concentration of Bax, Caspase-3, and Bcl-2 apoptotic markers. A comparison of the CP Group with Control, HTT, and DMSO Groups revealed that while the number of the positively-stained cells in Bax and Caspase-3 had increased, those of Bcl-2 had decreased. On the other hand, the number of the positively-stained cells had decreased in Bax and Caspase-3 while they increased in Bcl-2 as presented shown in Figs. 1-3.

Besides, the immunolabeling scores of the activated caspase-3, Bcl-2, and Bax were presented as Figs. S1-S3, respectively, in the supplementary information file. Histological damage scores of the lung tissues are presented in Table 3.

Table 3. Histological damage scores of the lung tissues [median (min-max)]

Groups	Hemorrhage	Edema	Congestion
Control	0 (0-0)	0 (0-0)	0 (0-0)
CP	3* (2-3)	3* (2-3)	3* (2-3)
HTT	0 (0-0)	0 (0-0)	0 (0-0)
CP+HTT	0 (0–0)	0 (0-1)	0 (0–1)
DMSO	0 (0-0)	0 (0-0)	0 (0-0)

*p<0.001 compared to Control, significant differences

In silico results for Caspase-3

In silico results for CP and Caspase-3 are given in Fig. S4. Besides the effects, CP and HT that were co-applied to the experimental rats upon Caspase-3 activities were determined, the results of which are given in Fig 4.

Summative results of the docking of CP and HT into Caspase-3 are presented in Table 4.

Table 4. Summative results of the docking of CP and HT into Caspase-3

Caspase-3			
	Active site residues	H-bond number	Negative binding energy (kcal/mol)
CP	Tyr204, Trp206, **Arg207*,** Ser205	**3 (2.92, 2.55, 2.86 Å)**	**-5.0**
CP& HT	Tyr204, Trp206, **Arg207***	**3 (2.72, 2.71, 3.02 Å)**	**-4.8**/-8.0

*An amino acid residue forming conventional hydrogen bonding

The effects of CP and HT that were co-applied to the rats upon the activity of Caspase-3 were determined thanks to in silico studies as presented in Fig. 4. A co-application of CP and HT showed a rise in the negative binding energy of the system (from -5.0 kcal/mol to -4.8 kcal/mol) for CP. Fig. 4.c displays a 2D view for modeling the binding of conventional hydrogen, along with an unfavorable positive-positive interaction and an unfavorable bump interaction, all of which occurred between CP and Caspase-3 whilst no carbon-hydrogen bond interaction occurred between CP and the Ser205 of Caspase-3. It was also revealed that the average length of three hydrogen bonds forming between CP and Arg207 had increased in the complex of CP-HT/Caspase-3 when compared to that of CP/Caspase-3 (Table 4). Moreover, two interactions occurred between HT and Arg207 in the CP-HT/Caspase-3 complex, one of which was a conventional hydrogen bond and the other was a carbon-hydrogen bond. The conventional hydrogen forming between HT and Arg207 (2.445 Å) was shorter than that of CP-Arg207 (Fig. 4.c).

In silico results for Bax

The results of the interaction of CP with Bax are given in Fig. S5. Besides, the effects of CP and HT upon the Bax activities, which were co-applied to the rats, were analyzed, whose results are displayed in Fig 5.

Summative results of the docking of CP and HT into Bax are presented in Table 5.

Table 5. Summative results of the docking of CP and HT into Bax

Bax			
	Active site residues	H-bond number	Negative binding energy (kcal/mol)
CP	**Gly39***	**1 (2.77 Å)**	**-4.6**
CP& HT	**Gly39***, Glu44, Ala46, Arg134	5 (2.28, 2.72, 2.39, 2.32, **2.79** Å)	**-4.6**/-6.1

*An amino acid residue forming conventional hydrogen bonding

With the aid of molecular docking studies, the effects of CP and HT that were co-applied to the rats upon Bax activities were determined as presented in Fig. 5. On the other hand, as was revealed by the co-application of CP and HT, no other change was observed in the negative binding energy of the CP/Bax complex (-4.6 kcal/mol) (Table 5). Like Fig. S5.c, Fig. 5.c displays a 2D view of the modeling of conventional hydrogen bond interaction between CP and Gly39 amino acid residue of Bax. In addition, the simultaneous docking of CP and HT into Bax revealed that the hydrogen bond length forming between Gly39 and CP in the CP-HT/Bax complex had increased from 2.77Å to 2.79Å when compared to the hydrogen bond length forming between Gly39 and CP in the CP/Bax complex (Table 5). Likewise, four conventional hydrogen bond interactions occurred between HT and Ala46, Glu44, and Arg134 amino acid residues whilst one Pi-Alkyl interaction occurred between Ala24 and HT in the CP/HT-Bax complex. However, the negative binding energy value of the CP/HT-Bax complex was found to be lower for HT than it was for CP (Table 5).

In silico results for Bcl-2

The results of the interaction of CP with Bcl-2 are given in Fig. S6. Apart from the effects of CP and HT that were co-applied to the rats upon Bcl-2 activities were determined via molecular docking studies, the results of which are presented in Fig 6.

Summative results of the docking of CP and HT into Bcl-2 are presented in Table 6.

Table 6. Summative results of the docking of CP and HT into Bcl-2

Bcl-2

	Active site residues	H-bond number	Negative binding energy (kcal/mol)
CP	**Tyr105, Phe109, Ala146**	No hydrogen bonds formed but two carbon-hydrogen interactions occurred	**-5.0**
CP& HT	**Phe109, Ala146** Ala97, Tyr199, Trp141	No hydrogen bonds formed for CP but three conventional hydrogen bond interactions occurred for HT	**-5.0**/-7.3

Thanks to molecular docking studies, the effects of CP and HT that were co-applied to the rats upon Bcl-2 activities were determined and the relevant results are presented in Fig. 6. The co-application of CP and HT showed no change in the negative binding energy for CP (-5.0 kcal/mol) (Table 6). Like Fig. S6.c, Fig. 6.c displays a 2D view of the modeling of carbon-hydrogen bond interactions occurring between CP and Phe109, Ala146 amino acid residues of Bcl-2. On the other hand, a simultaneous docking of CP and HT into Bcl-2 revealed that three new conventional hydrogen bonds had occurred between HT and Bcl-2 (Table 6). Besides, Fig. 6.c shows these interactions in the complex of CP-HT/Bcl-2: one Pi-Cation interaction between Arg134 and HT, two Pi-Pi Stacked interactions between Tyr105 and HT, one Pi-Pi T-shaped interaction between Phe101 and HT, one Pi-Alkyl interaction between Val105 and HT, and finally one Donor-Donor interaction between Trp141 and HT. Incidentally, the negative binding energy value of this complex for HT was found to be lower than the one found for CP (Table 6).

Discussion

This study aims to investigate whether or not HTT can recover CP-induced lung damage thanks to *in vivo* and *in silico* studies. In this study, in addition to apoptosis, severe damage was detected in the lung tissues of the CP Group, including structural defects, obstruction, bleeding areas, edema foci, and alveolar cell injuries, which are in agreement with the literature. Suddek *et al.*, showed that the rats given CP suffered damage and/or edema, congestion, macrophages infiltration, and neutrophilic in the interalveolar septa (Abd El-Ghafar et al., 2021). One other study reported alveolar cell injuries, alveolar septa thickness, erythrocytes, and polymorphonuclear cells in the alveolar lumen in histopathological examination of lung tissues in rats given CP (Şengül et al., 2017). Previous studies have also reported that CP causes apoptosis in the liver, kidney, bladder, and testicles (Can et al., 2022; Cengiz et al., 2020; Cengiz et al., 2019). However, no studies are available in the literature on CP-induced apoptosis. In our CP Group, while the number of the positively-stained cells in Bax and Caspase-3 had increased, those of Bcl-2 had decreased (Farrag et al., 2021).

HTT belongs to the Hypericaceae family that has been used thanks to its sedative, antiseptic, anti-helminthic, and anti-inflammatory effects (Can et al., 2022). Moreover, HTT is known for its phenolic and flavonoid compounds showing antioxidant and anti-apoptotic properties (Faraji et al., 2021). The anti-

oxidative activities of HTT can help suppress or decrease the side effects of many oxidative stress-induced diseases (Timraz et al., 2021). An experimental study reported that 100 mg/kg HTT achieved significant success in improving CP-induced testicular damage and apoptosis (Can et al., 2022). Also, Çetik *et al.* reported that CP-related cardiotoxicity, Bax, and Caspase-3 expressions decreased in CP + HTT Group while significantly increasing Bcl-2 expressions, suggesting that not only CP toxicity but also apoptosis intensity must have decreased in the cells (Cetik Yildiz et al., 2018). Our study is the first of its kind in the literature in that there are no studies available on the protective or curative effect of HTT upon lung injury.

The effects of CP-alone and CP combined with HTT upon Caspase-3 expression were evaluated via molecular docking results in addition to *in vivo* results. Considering Table 4, it was determined that three conventional hydrogen bonds had formed between Arg207 and CP thanks to the binding of CP to Caspase-3, the negative binding energy value of which was found to be -5.0 kcal/mol. On the other hand, our *in silico* studies showed that a combination of CP and HT also resulted in a decrease in the number of interactions made by CP with the catalytic amino acid residues of Caspase-3. However, the addition of HT increased the negative binding energy value from – 5.0 kcal/mol to -4.8 kcal/mol due to the formation of the CP/Caspase-3 complex besides increasing the average length of three hydrogen bonds that formed between CP and Arg207 increased. The fact that the negative binding energy value, an indication of the affinity of the protein to ligand, calculated after a co-application of CP-HT had increased when compared to that of the CP-alone meant that the affinity of Caspase-3 to CP had also decreased (Canofeni et al., 1994r, 2020; Gür, Cengiz, Kutlu, et al., 2021; Kassa et al., 2022). In other words, these results are suggestive of decreased Caspase-3 expression.

Consistent with the *in-vivo* results of this study, when the effects of CP-alone and a co-application of CP with HTT upon the expression of Bax were evaluated considering our molecular docking results, it was determined that while CP-alone had formed only one hydrogen bond with Bax, it had formed five with HT (Table 5). It was also determined that the hydrogen bond length that formed between CP and Gly39 when the CP-HT/Bax complex was created had increased compared to that of the CP/Bax complex, suggesting that the affinity of Bax to CP might have decreased. Besides, the formation of four new hydrogen bonds between HT and Bax in the CP-HT/Bax complex showed that Bax possessed a higher affinity for HT compared to CP. The negative binding energy values calculated appear to confirm these results, as presented in Table 5. In the formation of the CP-HT/Bax complex, this value was calculated as -6.1 kcal/mol for the docking of HT into Bax while it was calculated as -4.6 kcal/mol for the docking of CP into Bax. As a result, the co-application of CP with HT to the rats is understood to have caused a decrease in the affinity of Bax to CP, thus resulting in decreased Bax expressions. These results are consistent with the histopathological findings of this study.

When the results of the *in silico* studies carried out to investigate the effects of HT upon Bcl-2 expressions are evaluated, the affinity of Bcl-2 to CP is understood to have decreased considerably with the addition of HT. Furthermore, it was observed that Bcl-2 formed no conventional hydrogen bonds with CP in either of the CP/Bcl-2 and CP-HT/Bcl-2 complexes. On the other hand, it was also observed that

three new conventional hydrogen bond interactions had occurred between the catalytic amino acid residues of HT and Bcl-2 following the addition of HT. As far as the negative binding energy value obtained on account of the binding of HT to Bcl-2 in the CP-HT/Bcl-2 complex is concerned, this value was found to be considerably lower than that of the CP/Bcl-2 complex (-7.3 kcal/mol). This very low binding energy value and new hydrogen bond formations obtained for the CP-HT/Bcl-2 complex indicate that the affinity of Bcl-2 for HT must be very high compared to that for CP (Table 6). However, when HTT and CP were co-administered to the rats, it was observed that this application resulted in a positive effect upon the expressions of Bcl-2. In conclusion, this study suggests that the CP-related increase in Bcl-2 expressions can be prevented by the addition of HTT. These results are consistent with the histopathological results of the present study. The research team has shown in past studies that HTT works through anti-inflammatory and anti-apoptotic pathways to protect against a variety of experimentally produced tissue toxicities (Can et al., 2022; Cetik Yildiz et al., 2018). HTT may inadvertently prevent apoptosis. Additionally, by limiting the loss of GSH, it can boost antioxidant levels, reduce inflammatory processes by lowering intracellular Ca + + and ROS levels, and finally, reduced TNF- and ROS levels can inhibit apoptotic cell death (Yildiz et al., 2019).

Conclusion

Based on our in-vivo and in silico results, we suggest that HTT could be a potential candidate for eliminating the toxic side effects of CP upon the lungs. This study, however, also suggests that further scientific research is necessary to better evaluate the clinic applications of HTT on cancer sufferers.

Declarations

Funding This study was supported by Mardin Artuklu University - Coordination Unit of Scientific Research Project (MAU-BAP-15-SHMYO-23).

Author contributions the authors declare that all data were generated in-house and that no paper mill was used. SÇY conducted conceptualization, methodology, and experiment. CK contributed extract preparation, analytical tools, and data curation. VŞ contributed histopathological evaluations. BG and YO conducted molecular docking, software, and visualization. MC wrote the manuscript and contributed conceptualization, methodology, investigation formal analysis, investigation, Review & Editing Preparation, Writing - Original Draft, and Preparation. All authors read and approved the manuscript and all data were generated in-house and no paper mill was used.

Availability of data and materials All data can be obtained from the corresponding author as needed

Ethics approval It received approval from the Experimental Animal Ethics Committee of Eskişehir Osmangazi University (Protocol No. 444-1/2015).

Conflict of interest statement The authors report no declarations of interest.

Consent for publication The authors approve this submission.

Consent to participate Not applicable

References

1. Abd El-Ghafar OA, Hassanein EH, Sayed AM, Rashwan EK, Shalkami AGS, Mahmoud AM (2021) Acetovanillone prevents cyclophosphamide-induced acute lung injury by modulating PI3K/Akt/mTOR and Nrf2 signaling in rats. Phytother Res 35(8):4499–4510
2. Abdel-Latif GA, Elwahab AHA, Hasan RA, ElMongy NF, Ramzy MM, Louka ML, Schaalan MF (2020) A novel protective role of sacubitril/valsartan in cyclophosphamide induced lung injury in rats: impact of miRNA-150-3p on NF-κB/MAPK signaling trajectories. Sci Rep 10(1):1–17
3. Alzoubi KH, Abdel-Hafiz L, Khabour OF, El-Elimat T, Alzubi MA, Alali FQ (2020) Evaluation of the effect of Hypericum triquetrifolium turra on memory impairment induced by chronic psychosocial stress in rats: role of BDNF. Drug Des Devel Ther 14:5299
4. Badawi MS (2022) The protective effect of β-cryptoxanthin against cyclophosphamide-induced lung injury in adult male albino rats. Bull Natl Res Centre 46(1):1–9
5. Can S, Çetik Yıldız S, Keskin C, Şahintürk V, Cengiz M, Appak Başköy S, Ayhanci A, Akıncı G (2022) Investigation into the protective effects of Hypericum Triquetrifolium Turra seed against cyclophosphamide-induced testicular injury in Sprague Dawley rats. Drug Chem Toxicol 45(4):1679–1686
6. Canofeni S, Di Sario S, Mela J, Pilloton R (1994) Comparison of immobilisation procedures for development of an electrochemical PPO-based biosensor for on line monitoring of a depuration process. Anal Lett 27(9):1659–1669
7. Cengiz M, Sahinturk V, Yildiz SC, Şahin İK, Bilici N, Yaman SO, Altuner Y, Appak-Baskoy S, Ayhanci AJJ, Biology (2020) o. T. E. i. M.. Cyclophosphamide induced oxidative stress, lipid per oxidation, apoptosis and histopathological changes in rats: Protective role of boron. *62*,126574
8. Cengiz M, Yildiz SC, Demir C, Şahin İK, Teksoy Ö, Ayhanci A (2019) Hepato-preventive and anti-apoptotic role of boric acid against liver injury induced by cyclophosphamide. J Trace Elem Med Biol 53:1–7
9. Cetik Yildiz S, Keskin C, Şahintürk V, Ayhanci A (2018) Cardioprotective effects of Hypericum triquetrifolium Turra. against cyclophosphamide related cardiotoxicity in rats.Journal of Research in Pharmacy, *22*(3)
10. Cheemanapalli S, Pakala CMA, Chitta SK (2018) Design and screening of syringic acid analogues as BAX activators-An in silico approach to discover “BH3 mimetics”. Comput Biol Chem 74:49–62. https://doi.org/https://doi.org/10.1016/j.compbiolchem.2018.03.003
11. Chen L, Liu Y, Tang Z, Shi X, Song Z, Cao F, Wei P, Li M, Li X, Jiang D (2021) Improvements in estrogen deficiency-induced hypercholesterolemia by Hypericum perforatum L. extract are

associated with gut microbiota and related metabolites in ovariectomized (OVX) rats. Biomed Pharmacother 135:111131

12. Das UB, Mallick M, Debnath JM, Ghosh D (2002) J. A. j. o. a. Protective effect of ascorbic acid on cyclophosphamide-induced testicular gametogenic and androgenic disorders in male rats. *4*(3), 201–208
13. El-Kashef DH (2018) Role of venlafaxine in prevention of cyclophosphamide-induced lung toxicity and airway hyperactivity in rats. Environ Toxicol Pharmacol 58:70–76
14. Faraji N, Ganji A, Heshami N, Salehi I, Haddadian A, Shojaie S, Komaki A (2021) Hypolipidemic effects of Hypericum Scabrum extract on the serum lipid profile and obesity in high-fat diet fed rats. Hum Antib 29(1):55–61
15. Farrag IM, Belal A, Al Badawi MH, Abdelhady AA, Galala A, El-Sharkawy FM, El-Dahshan A, Mehany AB (2021) Antiproliferative, apoptotic effects and suppression of oxidative stress of quercetin against induced toxicity in lung cancer cells of rats: In vitro and in vivo study. J Cancer 12(17):5249
16. Gür B (2020) Determination of the pH-dependent immobilization efficacy of α-glycosidase and its catalytic performance on SnO2:Sb/ITO thin films. Biochem Eng J 163:107758. https://doi.org/https://doi.org/10.1016/j.bej.2020.107758
17. Gür F, Cengiz M, Gür B (2021) Alternations in nuclear factor kappa beta activity (NF-kB) in the rat brain due to long-term use of atomoxetine for treating ADHD: In vivo and in silico studies. Biochem Biophys Res Commun 534:927–932
18. Gür F, Cengiz M, Kutlu HM, Cengiz BP, Ayhancı A (2021) Molecular docking analyses of Escin as regards cyclophosphamide-induced cardiotoxicity: In vivo and in Silico studies. Toxicol Appl Pharmcol 411:115386. https://doi.org/https://doi.org/10.1016/j.taap.2020.115386
19. Gür F, Gür B, Erkayman B, Halıcı Z, Karakoç A (2020) Investigation of serum and brain superoxide dismutase levels depending on atomoxetine used in attention-deficit/hyperactivity disorder treatment: A combination of in vivo and molecular docking studies. Bioorg Chem 105:104435. https://doi.org/https://doi.org/10.1016/j.bioorg.2020.104435
20. Habibi E, Shokrzadeh M, Ahmadi A, Chabra A, Naghshvar F, Haghi-Aminjan H, Salehi F (2020) Pulmonoprotective action of Zataria multiflora ethanolic extract on cyclophosphamide-induced oxidative lung toxicity in mice. Chin J Integr Med 26(10):754–761
21. Ibaokurgil F, Yildirim BA, Yildirim S (2022) Effects of Hypericum scabrum L. essential oil on wound healing in streptozotocin-induced diabetic rats.Cutaneous and Ocular Toxicology,1–8
22. Kassa SB, Taslimi P, Özel Ş, Gür B, Gülçin İ, Onganer Y (2022) Effects of some phenolic compounds on the inhibition of α-glycosidase enzyme-immobilized on Pluronic®F127 micelles: An in vitro and in silico study. Colloids Surf A 632:127839. https://doi.org/https://doi.org/10.1016/j.colsurfa.2021.127839
23. Kaya ED, Türkhan A, Gür F, Gür B (2021) A novel method for explaining the product inhibition mechanisms via molecular docking: inhibition studies for tyrosinase from Agaricus bisporus.Journal of Biomolecular Structure and Dynamics,1–14

24. Kostal J (2016) Computational Chemistry in Predictive Toxicology: status quo et quo vadis? Advances in molecular toxicology, vol 10. Elsevier, pp 139–186
25. Liu J, Huang X, Hu S, He H, Meng Z (2019) Dexmedetomidine attenuates lipopolysaccharide induced acute lung injury in rats by inhibition of caveolin-1 downstream signaling. Biomed Pharmacother 118:109314. https://doi.org/https://doi.org/10.1016/j.biopha.2019.109314
26. Manzullo EF, Escalante CP (2002) Research into fatigue. Hematology/Oncology Clin 16(3):619–628
27. Mohamed MT, Zaitone SA, Ahmed A, Mehanna ET, El-Sayed NM (2020) Raspberry ketones attenuate cyclophosphamide-induced pulmonary toxicity in mice through inhibition of oxidative stress and NF-KB pathway. Antioxidants 9(11):1168
28. Mustafa YS, Maulood KA (2019) Protective Effect of Hypericum Triquetrifolium Aqueous Extract on Biochemical and Histopathological Parameters in Hyperlipidemic Male Rats. Kirkuk Univ Journal-Scientific Stud 14(4):63–88
29. Naraoka T, Sumi T, Keira Y, Nakata H, Chiba H (2021) Epirubicin and Cyclophosphamide–induced Acute Fibrinous and Organizing Pneumonia. Am J Respir Crit Care Med 204(8):e92–e93
30. Saghir SA, Alharbi SA, Al-Garadi MA, Al-Gabri N, Rady HY, Olama NK, Abdulghani MA, Hroob A, Almaiman AM, Bin-Jumah M (2020) Curcumin prevents cyclophosphamide-induced lung injury in rats by suppressing oxidative stress and apoptosis. Processes 8(2):127
31. Shityakov S, Förster C (2014) In silico predictive model to determine vector-mediated transport properties for the blood–brain barrier choline transporter. *Advances and Applications in Bioinformatics and Chemistry*, *2014*, 23–36. https://doi.org/10.2147/AABC.S63749
32. Siddiqui S, Upadhyay S, Ahmad I, Hussain A, Ahamed M (2021) Cytotoxicity of Moringa oleifera fruits on human liver cancer and molecular docking analysis of bioactive constituents against caspase-3 enzyme. J Food Biochem 45(5) Article e13720. https://doi.org/10.1111/jfbc.13720
33. Silva AR, Taofiq O, Ferreira IC, Barros L (2021) Hypericum genus cosmeceutical application–A decade comprehensive review on its multifunctional biological properties. Ind Crops Prod 159:113053
34. Sinha R, Vidyarthi AS (2011) A molecular docking study of anticancer drug paclitaxel and its analogues
35. Suvarna KS, Layton C, Bancroft JD (2018) Bancroft's theory and practice of histological techniques E-Book. Elsevier health sciences
36. Şengül E, Gelen V, Gedikli S, Özkanlar S, Gür C, Çelebi F, Çınar A (2017) The protective effect of quercetin on cyclophosphamide-Induced lung toxicity in rats. Biomed Pharmacother 92:303–307
37. Timraz NZ, El-Bassossy HM, Ibrahim SR, El-Halawany AM, Aljohani OS, Abdallah HM (2021) Vasodilating effect of Hypericum revolutum (Vahl)(Clusiaceae) methanol extract in rats. Trop J Pharm Res 20(5):1003–1007
38. Toker Z (2009) Variation of total hypericin, phenolic and flavonoid compounds in Hypericum triquetrifolium during its phenological cycle. Pharm Biol 47(4):285–288

39. Trott O, Olson AJ (2010) AutoDock Vina: improving the speed and accuracy of docking with a new scoring function, efficient optimization, and multithreading. J Comput Chem 31(2):455–461
40. Yildiz SC, Keskin C, Sahintürk V, Ayhanci A (2019) A histopathological, immunohistochemical and biochemical investigation on the in vitro antioxidant, myeloprotective, hematoprotective and hepatoprotective effects of Hypericum triquetrifolium seed extract against cyclophosphamide-induced toxicity. *Brazilian Archives of Biology and Technology*, *62*

Supplementary Information

The Supplementary Information file is not available with this version

Figures

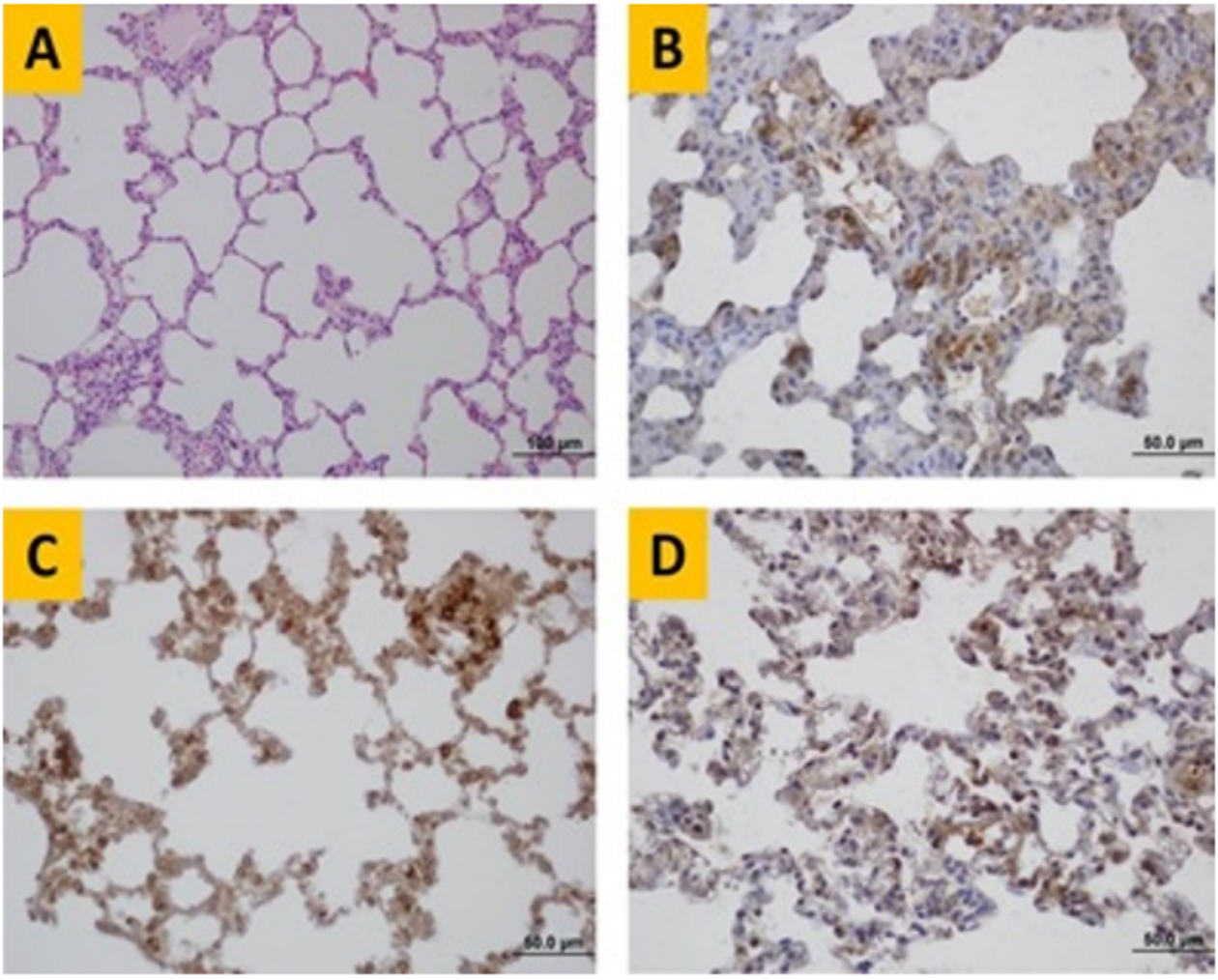

Figure 1

(A) Images of Control, HTT, and DMSO groups (B) Caspase-3 (C) Bcl-2 (D) Bax. Bars are between 50-100 µm

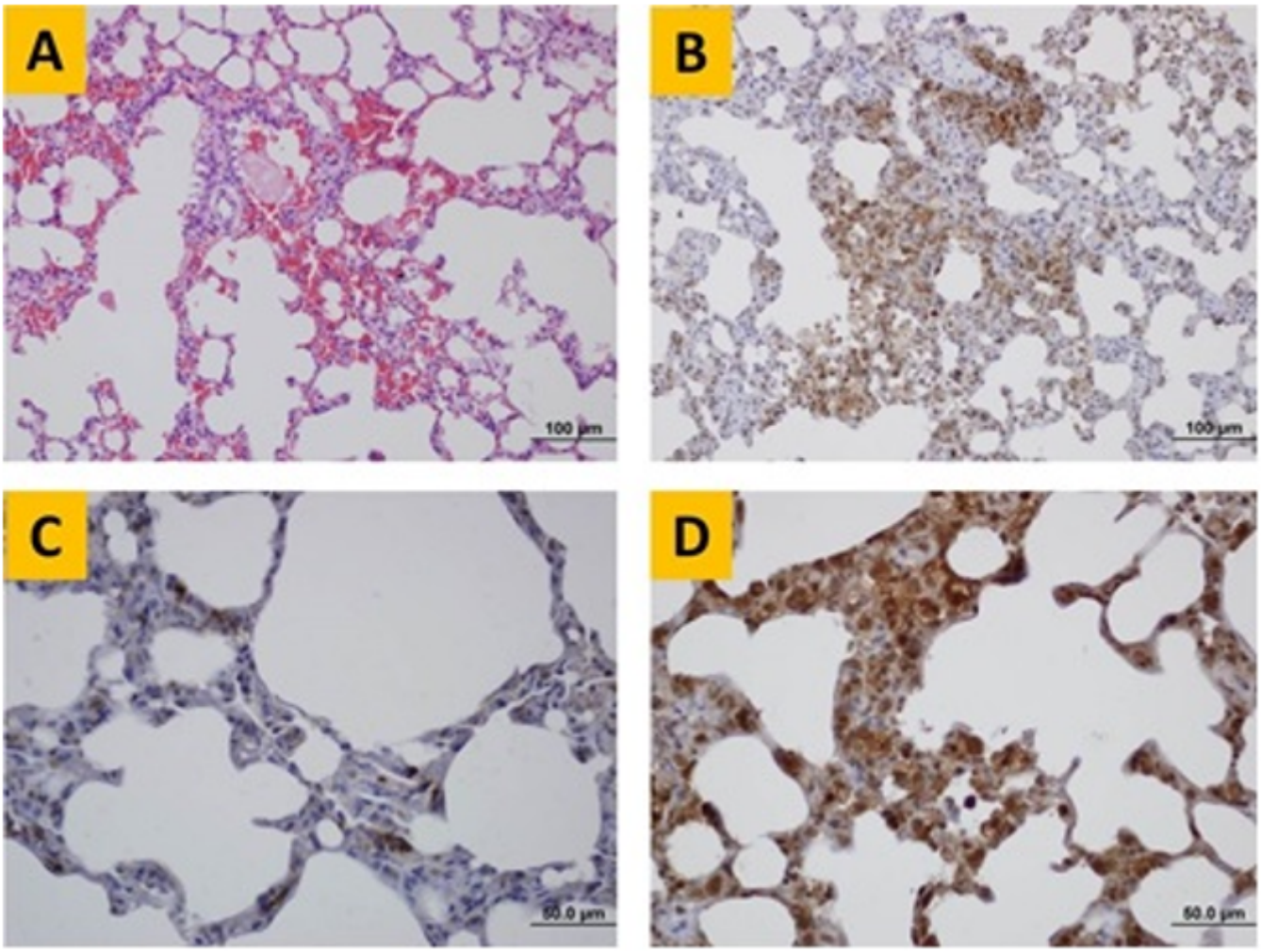

Figure 2

(A) Images of CP (B) Caspase-3 (C) Bcl-2 (D) Bax groups. Bars are between 50-100 µm

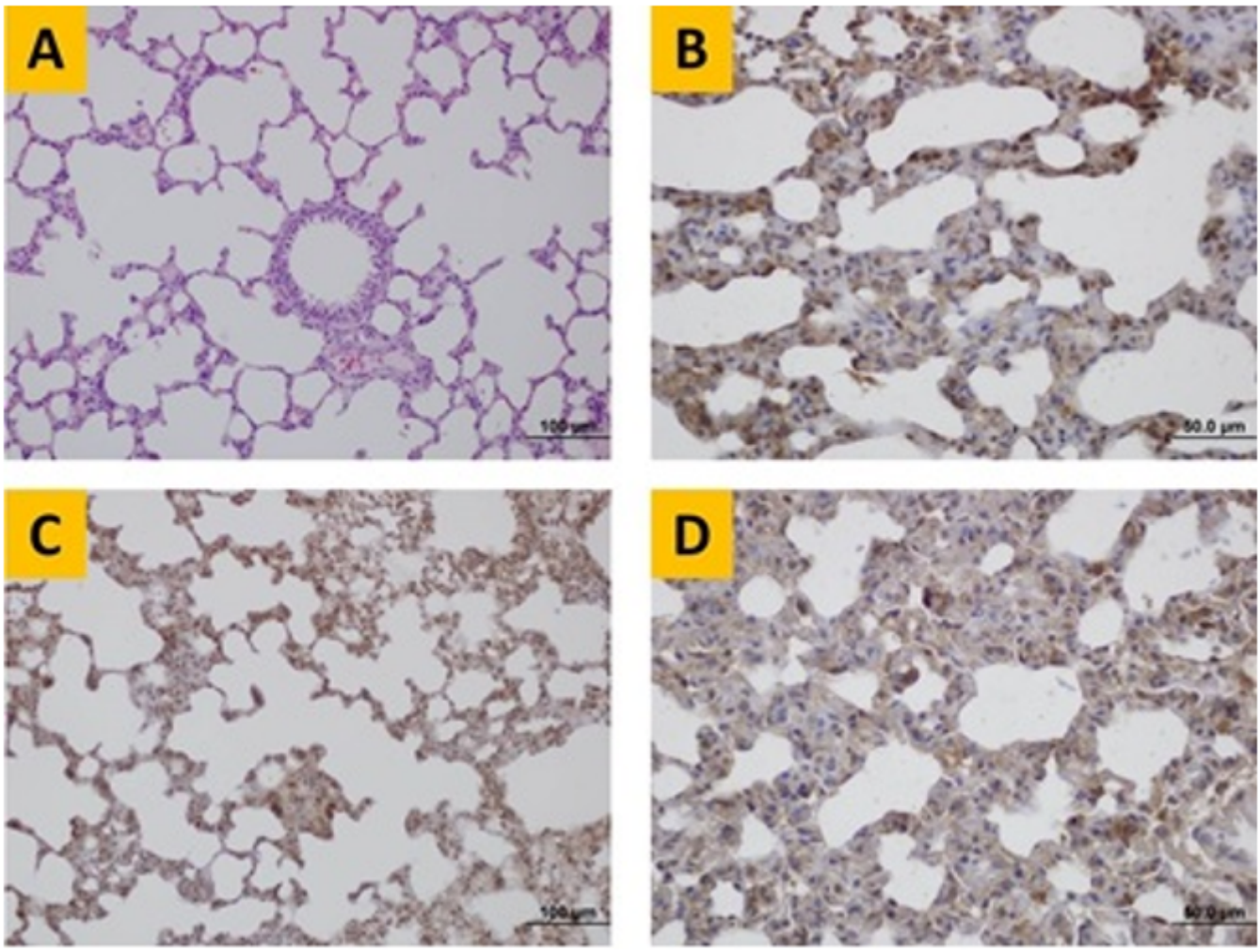

Figure 3

(A) Images of CP+HTT (B) Caspase-3 (C) Bcl-2 (D) Bax groups. Bars are 50-100 µm

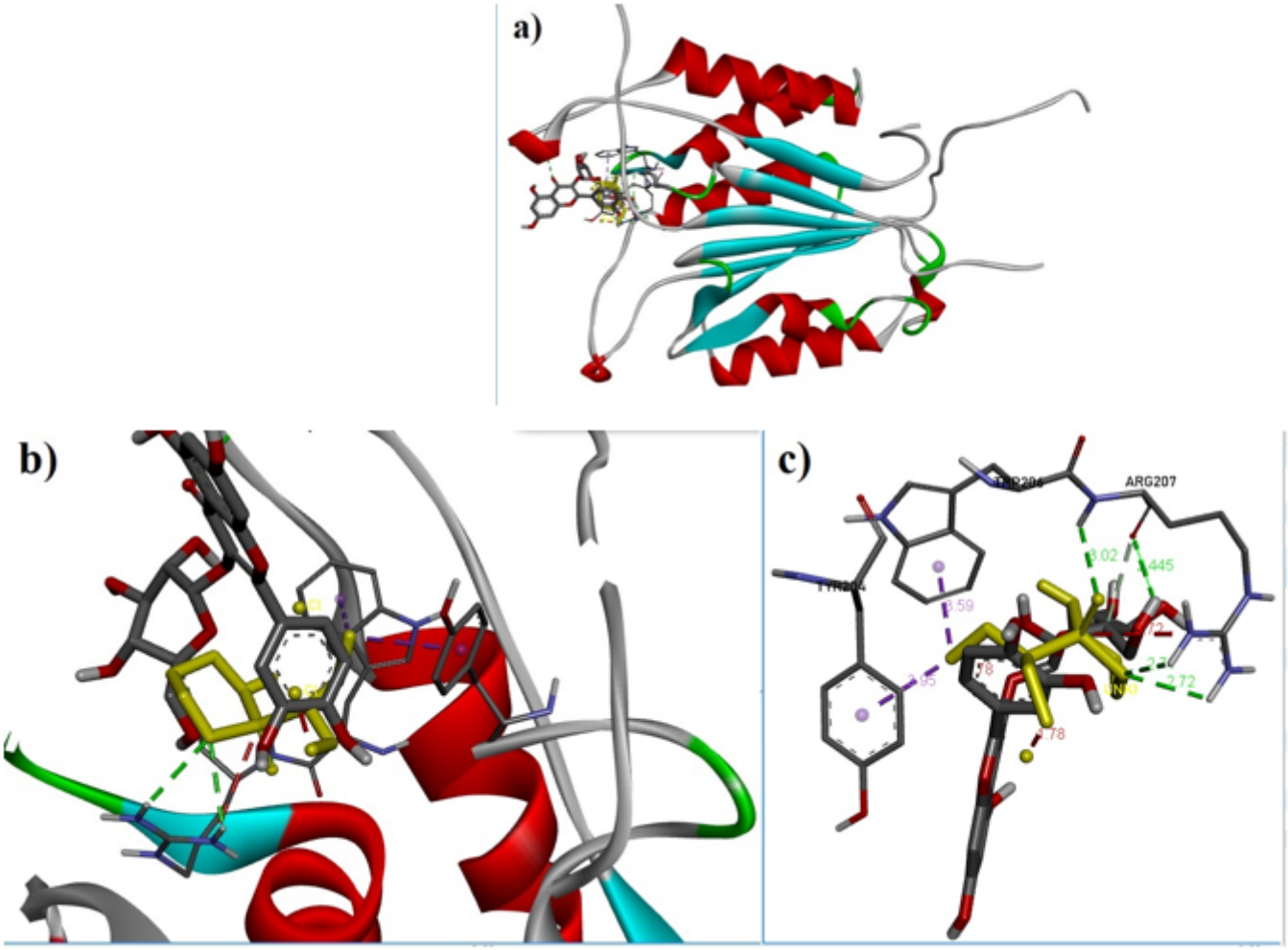

Figure 4

Results of the docking of CP+HT into Caspase-3: (a) 3D view showing CP (the yellow stick structure) interacting with Caspase-3 once CP+HT were docked into Caspase-3 (b) 3D view showing CP interacting with Caspase-3 once HT (The yellow stick structure) were docked into Caspase-3, (c) 2D view displaying the CP+HT interacting with the amino acid residues of Caspase-3

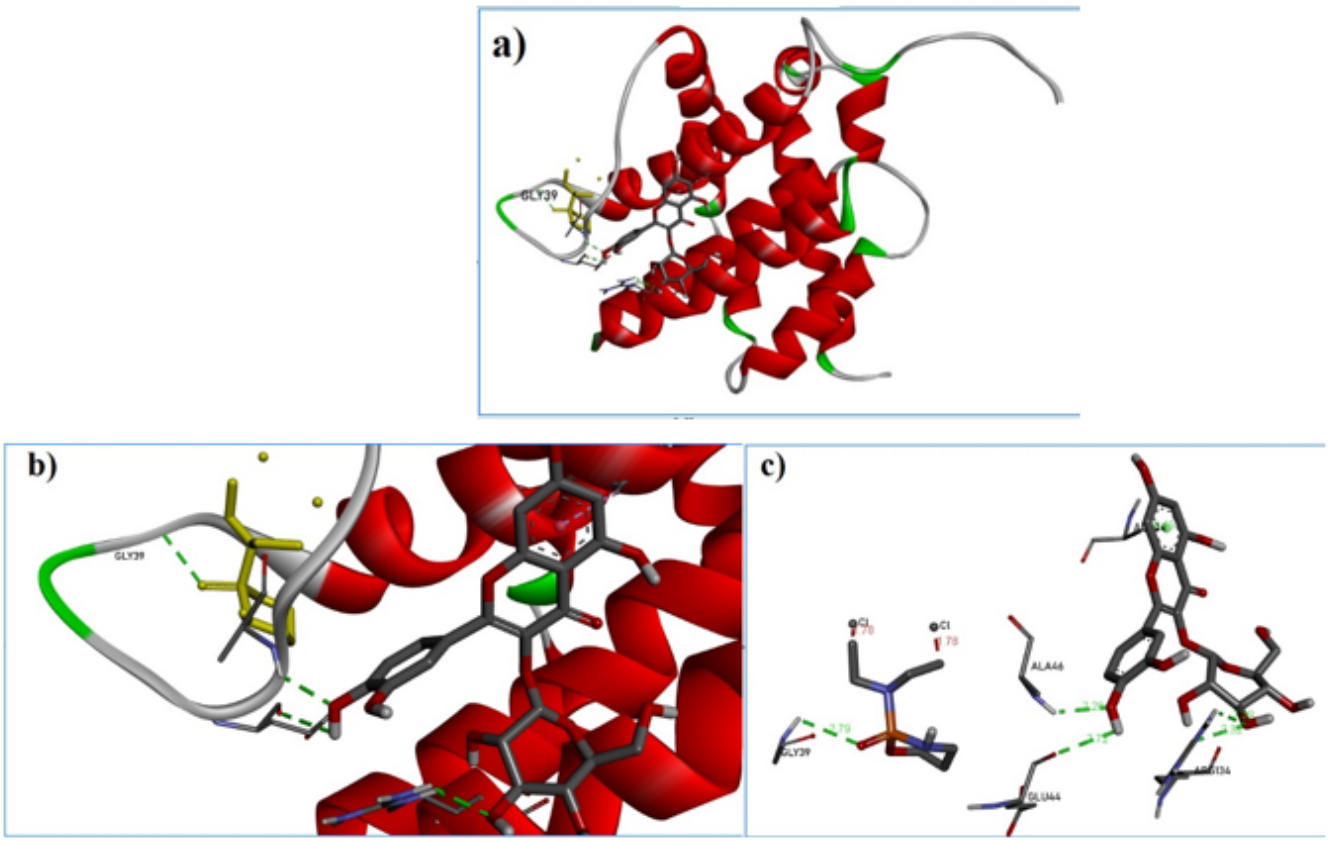

Figure 5

Result of the docking of CP+HT into Bax: (a) 3D view of the interaction between CP (The yellow stick structure) and Bax once CP+HT had been docked into Bax (b) 3D zoomed view displaying the interaction occurring between CP and Caspase-3 once HT (The yellow stick structure) were docked into Bax, (c) 2D binding mode view of CP+HT with the amino acid residues of Bax

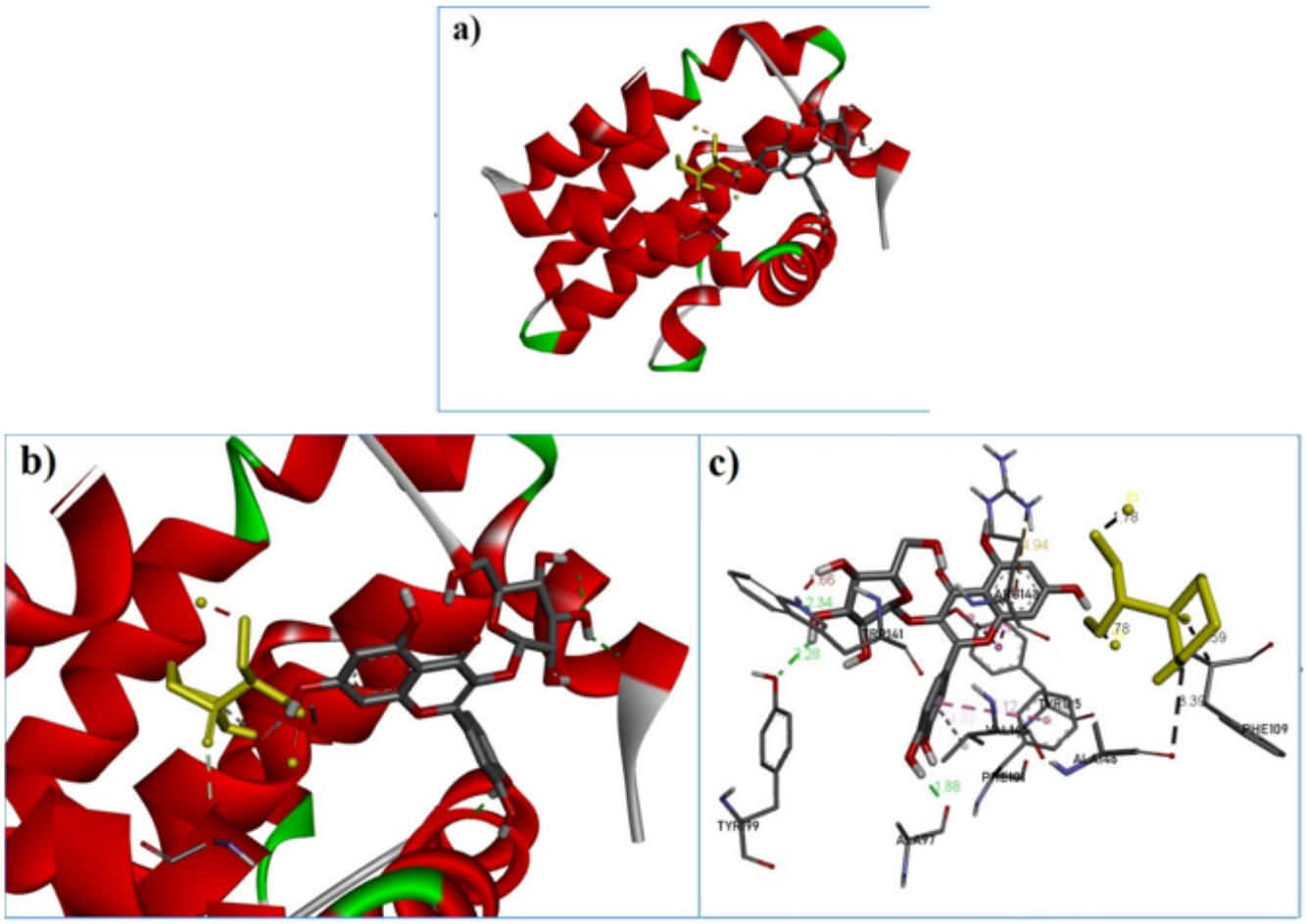

Figure 6

Results of the docking of CP+HT into Bcl-2: (a) 3D view of the interaction between CP (The yellow stick structure) and Bcl-2 once CP+HT had been docked into Bcl-2 (b) 3D zoomed view of the interaction between CP and Bcl-2 once HT (The stick structure) had been docked into Bcl-2, (c) 2D view displaying CP+HT (The yellow stick structure only for CP) interacting with the amino acid residues of Bcl-2

Supplementary Files

This is a list of supplementary files associated with this preprint. Click to download.

- GraphicalAbstract.jpg
- Highlights.docx